Title

Reactions of C+ + Cl−, Br−, and I−—A comparison of theory and experiment

Journal

The Journal of Chemical Physics, 151(24)

ISSN

0021-9606

Authors

Sawyer, Jordan C
Hedvall, Patrik
Miller, Thomas M
et al.

Publication Date

2019-12-28

DOI

10.1063/1.5126689

Peer reviewed

Reactions of $C^+ + Cl^-, Br^-,$ and I^- – A Comparison of Theory and Experiment

Jordan C. Sawyer[1], Patrik Hedvall[2], Thomas M. Miller[3], Kenneth W. Engeling[4], Åsa Larson[2*], Ann E Orel[5], Albert A. Viggiano[6], and Nicholas S. Shuman[6*]

1. *NRC postdoc at Air Force Research Laboratory, Space Vehicles Directorate, Kirtland Air Force Base, New Mexico 87117, USA*

2. *Department of Physics, Stockholm University, AlbaNova University Center, S-10691 Stockholm, Sweden*

3. *Boston College Institute for Scientific Research, Boston, MA 02549*

4. *Department of Nuclear Engineering and Radiological Sciences, University of Michigan, Ann Arbor MI 48109, USA*

5. *Department of Chemical Engineering, University of California, Davis, Davis, CA 95616, USA*

6. *Air Force Research Laboratory, Space Vehicles Directorate, Kirtland Air Force Base, New Mexico 87117, USA*

Abstract

Rate constants for the reactions of $C^+ + Cl^-, Br^-,$ and I^- were measured at 300 K using the variable electron and neutral density electron attachment mass spectrometry technique in a flowing afterglow Langmuir probe apparatus. Upper bounds of $< 10^{-8}$ cm^3 s^{-1} were found for reaction of C^+ with Br^- and I^-, and a rate constant of $4.2 \pm 1.1 \times 10^{-9}$ cm^3 s^{-1} was measured for reaction with Cl^-. The $C^+ + Cl^-$ mutual neutralization reaction was studied theoretically from first principles and a rate constant of 3.9×10^{-10} cm^3 s^{-1}, an order of magnitude smaller than experiment, was obtained with spin-orbit interactions included using a semi-empirical model. The discrepancy between the measured and calculated rate constants could be explained by the fact that in the experiment the total loss of C^+ ions was measured, while the theoretical treatment did not include the associative ionization channel. The charge transfer was found to take place at small internuclear distances and the spin-orbit interaction was found to have a minor effect on the rate constant.

Introduction

Charge transfer between positive and negative ions, termed mutual neutralization (MN), is one of the fundamental plasma interactions limiting the density in ion-ion plasmas occurring in environments such as the lower ionosphere[1], flames[2], interstellar plasmas[3, 4], and non-equilibrium discharges.[5] Accurate experimental measurement of MN at thermal energies has been difficult. The first quantitative rate constants were measured using stationary afterglows, but suffered from no or limited mass detection as well as pressure effects likely leading to inaccuracies in Langmuir probe measurements.[6-10] In the early 1970's, thermal rate constants for a number of systems involving small, ionospherically-relevant ions on the order of several $\times 10^{-7}$ cm^3 s^{-1} were extrapolated from merged beam experiments conducted at collision energies above 0.1 eV.[11-14] Values determined using a flowing afterglow apparatus several years later were about an order of magnitude lower, around 5×10^{-8} cm^3 s^{-1}, and these were accepted as the first accurate measurements.[4, 15] Only about a dozen systems were investigated in this manner, as little variation in rate constants was observed and the flowing afterglow method did not offer a means of determining the neutral product distribution. Little work followed until the late 2000's when two experiments began reporting MN kinetics data. An advanced merged beam technique accurately controlled collision energies down to ~0.01 eV, i.e. thermal energies, initially only for the $H^+ + H^-$ system,[16, 17] but more recently for a wider range of atom-atom systems reporting both cross-sections and product information.[18, 19] Separately, an updated flowing afterglow methodology, developed by our group, termed variable electron and neutral density attachment mass spectrometry (VENDAMS)[20] provided an order of magnitude lower detection limit than the traditional flowing afterglow technique, allowed access to a broader range of systems,[21, 22] as well as limited product information.[23] Recent efforts using VENDAMS have focused on atom-atom MN systems.[24-26]

MN systems involving 4 or more atoms show little variation in rate constants, and what variation is seen is largely explained by the relative velocity of the particles indicated by the reduced mass of the system.[21] Systems involving three atoms also show little variation, but tend to have room temperature rate constants about one half as large as the polyatomic systems. Atom-atom MN reactions, however, show a wide range in their rate constants, varying by at least a factor of 100 (our dynamic range) at room temperature.[26] This system-size dependent behavior can be rationalized by the fundamental nature of the MN process.

The two ions approach along a potential dominated by the Coulomb attraction, but in order to exit to products must cross to a neutral surface. The crossing probability to a particular state is a function of the coupling between that state and the initial Coulomb surface. For polyatomic systems a large number of product electronic and vibrational states exist, and in general some subset of those crossings will most likely be favorable, dominating reactivity and blurring out the system-specific aspects of the reaction. The number of crossings decreases with the number of modes in the system, until for atom-atom systems the possible product electronic states become sparse, and the specifics of those crossings become more important such that they dominate the reactivity.

Atom-atom systems then provide a more promising avenue than polyatomic systems for comparing theoretical treatments of MN to experiment. Because *ab initio* treatments must consider many excited states out to large internuclear distances, only systems with few electrons and few degrees of freedom are practical to calculate.[16, 27-33] It is then sensible to validate theoretical methods by comparison to experimental MN results of atom-atom systems. To date, there is limited overlap between systems that have received both theoretical and experimental treatments. Studies of , $He^+ + H^-$ [12] have provided such overlap at higher energies, and studies of $H^+ + H^-$ [8, 13] and $H^+ + Cl^-$ [34] at thermal energies. In the case of the latter, theory and experiment were only superficially consistent, with a large inconsistency in the isotope effect on the thermal rate constant.[24, 20] The large energy and geometrical phase space and coupling to electronically excited state(s) that are inherent in MN reactions present significant difficulties in *ab initio* and fully quantum mechanical studies. Meanwhile, the double electrostatic ion storage ring experiment (DESIREE) located at Stockholm University is beginning to provide data on MN processes, offering a revolution in the field analogous to that seen for dissociative recombination provided by magnetic ion storage rings in the 1990's and 2000's. There is need to advance and validate theoretical treatments of MN in order to understand and analyze results provided using DESIREE. Here we present results on an atom-atom MN system, $C^+ + Cl^-$, which is accessible to both the VENDAMS method and *ab initio* treatment.

In particular, spin-orbit coupling has not yet been accounted for in the theoretical treatment which sets limitation on the size of the system that can be studied accurately. Additionally, the theory in general does not include the possibility of autoionization. In most theoretical mutual neutralization studies, the non-adiabatic interactions between a finite number of electronic bound states have been considered (often using a strict diabatic representation). The non-adiabatic interactions between these bound states and the ionization continuum have so far been neglected. Additionally, the electronic states involved in the mutual neutralization reaction might interact with electronic resonant states coupled directly with the ionization continuum through electronic interactions. These electronic resonant states are described using a diabatic (or quasi-diabatic) representation and it is not unambiguous how to connect these states with the adiabatic bound states important for the mutual neutralization reaction at large internuclear distances. Autoionization has so far only been included in the case of $He^+ + H^-$ [12] and $H^+ + F^-$,[9] where the loss due to autoionization was considered using local complex potentials of electronic resonant states. In the case of $He^+ + H^-$ all states involved were at small internculear distances resonant states due to the fact that the ion-pair state is embedded in the ionization continuum of HeH^+. For $H^+ + F^-$, quasidiabatic states were used throughout and the ion-pair state crossed the HF^+ ion potential at small distances and becomes an electronic resonant state.

In the present study we provide a new point of comparison between theoretical and experimental thermal rate constants of the reaction of $C^+ + Cl^-$ at 300 K. In the experiment, the total rate constant accounting for depletion of C^+ ions is measured, including mutual neutralization and associative ionization. Potential energy curves for the five lowest electronic states of the $^2\Sigma^+$ symmetry and the seven lowest electronic states for the $^2\Pi$ symmetry and the non-adiabatic couplings between these states have been calculated. These are states associated with the $C(^3P) + Cl(^2P)$, $C(^1D) + Cl(^2P)$, $C(^1S) + Cl(^2P)$ and $C^+ + Cl^-$ asymptotic limits. It was found that the avoided

curve crossings occur at relatively small internuclear distances (< 6 a_0). The importance of the spin-orbit coupling has been investigated using a semi-empirical method,[35, 36] where the spin-orbit Hamiltonian was approximated using the asymptotic atomic spin-orbit coupling parameter of $Cl(^2P)$. Then all doublet and quintet molecular states associated with the included asymptotic limits have to be considered in the model. The calculated results are compared with the measured rate constant for $C^+ + Cl^-$. For the systems $C^+ + Br^-$ and $C^+ + I^-$ measured upper limits of the rate constants are reported.

Experiment

The Air Force Research Laboratory's flowing afterglow Langmuir probe apparatus and the variable electron neutral density attachment mass spectrometry (VENDAMS) technique for measuring mutual neutralization rate constants have been described in prior works.[25, 26, 37] A schematic of the FALP apparatus with the reaction scheme used to measure the rate constant of $C^+ + I^-$ is shown in Fig. 1. Helium (99.999%, Matheson) is purified further by passing through a Mono Torr phase II purifier (SAES Pure Gas, Inc.). The helium flow, 13 std. L min^{-1}, entered the FALP through a 2.5 cm diameter upstream inlet arm. A weakly ionized plasma was formed in the inlet arm via a movable microwave discharge and flowed into the 7.3-cm internal-diameter flow tube. The plasma consisted of He^+, He_2^+, and e^- with some of the neutrals being metastable helium, He^*. The nascent distribution of these species at the beginning of the flow tube is highly dependent on the location of the microwave discharge on the He inlet arm.[25] A few cm downstream Ar and CO were added to the afterglow. He_2^+ and He^* were rapidly converted to Ar^+ and CO^+. C^+ was formed via the reaction $He^+ + CO \rightarrow C^+ + O + He$. Several cm downstream the plasma consisted primarily of C^+, CO^+, Ar^+, and e^- with < 1% of impurity ions due to trace air and water in the He. Halfway along the flow tube a fast-attaching ($k_a > 1 \times 10^{-7}$ cm^3 s^{-1}) neutral precursor was added to the flow through 5 hollow needles pointing radially toward the flow tube axis. In this work, CCl_4, CF_2Br_2, and C_2F_3I were the neutral precursors used to make the atomic halide anions Cl^-, Br^-, and I^-, respectively.[38, 39] All flows were metered using mass flow controllers (MKS Instruments).

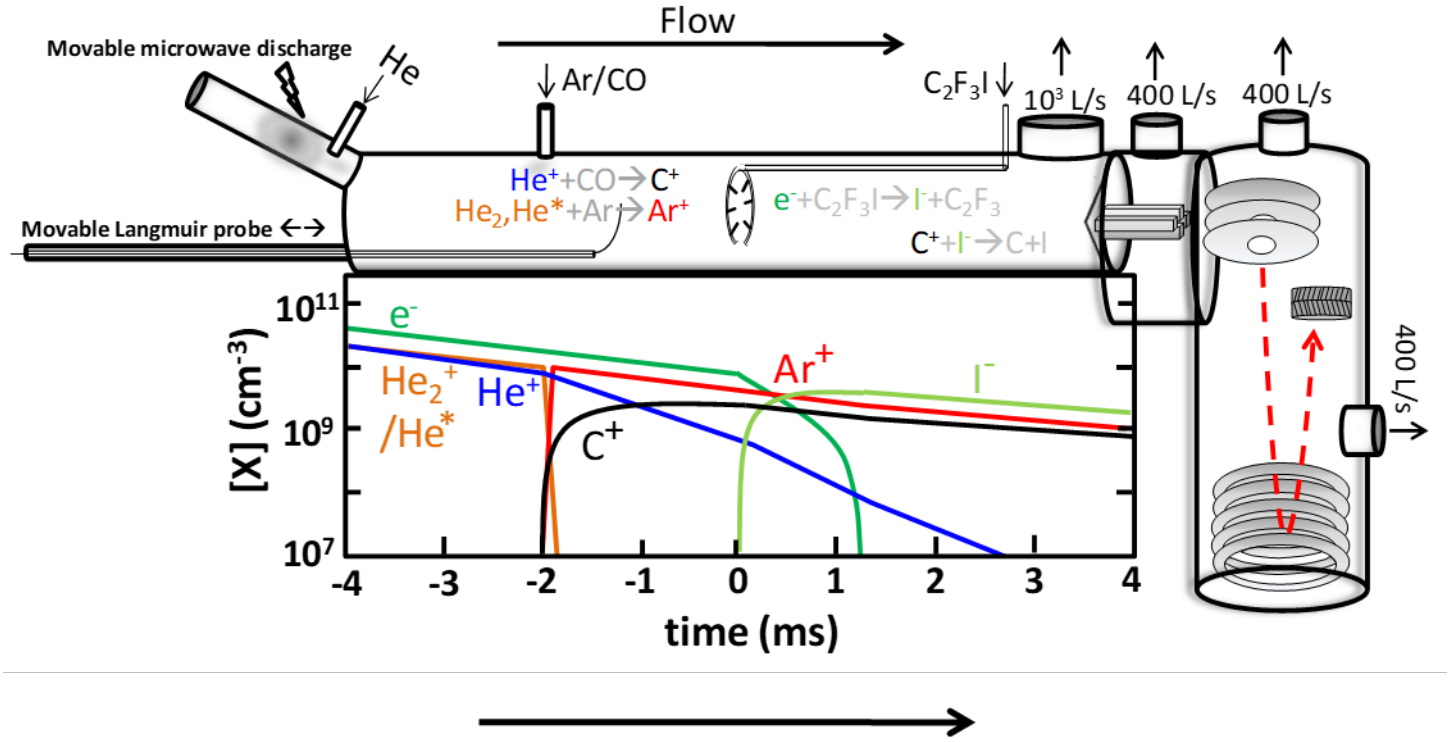

FIG. 1 Schematic of the FALP with VENDAMS scheme for measuring $C^+ + I^- \rightarrow C + I$ along with modeled concentrations of key species as a function of time relative to addition of the attaching gas as well as the approximate distance along the flow tube.

Ions on the axis of the flow were sampled through a 330-μm aperture in a truncated nosecone at the downstream end of the flow tube. Most of the gas was pumped out of the system using a Roots pump. Ions sampled through the nosecone were transported using a rectilinear quadrupole ion guide operated at 8.9 MHz to an orthogonally-accelerated reflectron time-of-flight mass spectrometer (TOF-MS). The transmission through the quadrupole ion guide has a mass-dependence. In order to establish mass-discrimination between C^+ and Ar^+, an ion-molecule rate constant measurement for the reaction of $Ar^+ + CH_4$ was performed by adding CH_4 through the reactant inlet. By fitting the CH_3^+ products over several runs with varying initial electron density a reasonable estimate for the C^+ to Ar^+ mass discrimination was obtained. C^+ was detected less efficiently than Ar^+ by a factor of 3. Higher mass ions have little discrimination.

The absolute electron density in the plasma along the axis of the flow was measured using a cylindrical Langmuir probe (0.025-mm diameter tungsten wire, 7.6-mm long). The Langmuir probe could be moved to make measurements over the entire length of the flow tube. The initial plasma density, $[e]_0$, just before the radial reactant inlet can be set between ~10^8 cm^{-3} and ~5 × 10^{10} cm^{-3} by changing the microwave cavity position. The lower limit is set by the resolution of the Langmuir probe and the upper limit is largely dominated by ambipolar diffusive losses. By pulsing the microwave discharge and measuring the time of arrival of the disturbance at various

axial locations the ion velocity could be measured. In this work, a typical ion velocity was 11,000 cm s^{-1} for the buffer gas conditions of 300 K and 0.8 Torr. A reaction time of ~4 ms was obtained for the reaction zone from the needle inlet to the nosecone.

Previously we developed a variation of our VENDAMS technique to measure MN rate constants in systems that are particularly sensitive to the nascent distribution of He^+ and Ar^+.[24] In this technique we maintain a constant initial electron density at the reactant inlet and vary the concentration of our attaching neutral precursor: CCl_4, CF_2Br_2, or C_2F_3I. Varying the neutral precursor concentration effectively varies the concentration of the atomic halide anion species ($X^- = Cl^-, Br^-, \text{or } I^-$) along the length of the flow tube. The thermal rate constant for the reaction of interest, $C^+ + X^-$, can then be derived relative to that of $Ar^+ + X^-$. Since the later values have been previously measured, absolute numbers can be derived. Rate constants are derived by fitting the relative ion abundances of Ar^+, C^+, and any substantial polyatomic cation species present in the flow as the neutral precursor concentration is varied. A minimum of two measurements were taken for each probed reaction at initial electron densities of $\sim 3 \text{ and } 5 \times 10^{10}$ cm^{-3} as a consistency check and to better establish uncertainty in the rate constants.

Data and Analysis

Representative data sets for the VENDAMS measurements of $C^+ + X^-$ are shown in Fig. 2. Measured relative ion abundances as a function of neutral precursor concentration are shown as the points while the dashed lines represent uncertainty bounds from Monte Carlo simulations. Rate constants for all previously studied reactions could vary within their reported uncertainty limits in the Monte Carlo simulations. After a ~10^{10} cm^{-3} concentration of the neutral precursor is added the plasma transitions from ion-electron to ion-ion. This gives the polyatomic cations a rising slope due to mitigating dissociative recombination. The transition at ~10^{10} cm^{-3} concentration roughly marks where the relative abundances of Ar^+ and C^+ become sensitive to the mutual neutralization reaction. Further increasing the neutral precursor concentration beyond this point decreases the physical onset time of the transition to an ion-ion plasma leading to an increased mutual neutralization reaction time. Comparing the slopes of the Ar^+ and C^+ curves for each data set gives some hint at the relative mutual neutralization rates. In the Cl^- and Br^- data sets the Ar^+ and C^+ the curves are both relatively flat with increasing neutral precursor concentration indicating that the C^+ MN rate constant is similar to that of the Ar^+ MN rate constant with the respective anion (for both $Ar^+ + Cl^-$ and $Ar^+ + Br^-$, $k_{300K} \sim 5\times10^{-9}$ cm^3 s^{-1}).[26] In the I^- data set the Ar^+ and C^+ curve have negative and positive slopes, respectively, indicating that the $C^+ + I^-$ reaction proceeds at a significantly slower rate than $Ar^+ + I^-$ (for which $k_{300K} = 2 \pm 0.5 \times10^{-8}$ cm^3 s^{-1}).[26] For clarity data and fits for only the most relevant cations in each set are shown in Fig. 2, but all cation species that were present in concentrations at least on the same order of magnitude as those shown were included in the modeling. A broad range of possible chemistry was considered in the modeling including: reaction of ions with the electron attaching precursor gas, secondary chemistry with neutral co-products of electron attachment or ion-molecule reaction, dissociative recombination of all polyatomic cations, and mutual neutralization of all cations with the dominant anion. Where rate constants for these processes are not constrained by the literature, they are varied across a

wide range, up to the calculated collision rate for ion-molecule processes, up to 10^{-6} cm^3 s^{-1} for dissociative recombination processes, and up to 5×10^{-7} cm^3 s^{-1} for mutual neutralization processes.

The derived rate constants for the reactions of C^+ with the atomic halide anions Cl^-, Br^-, and I^- at 300 K are shown in Table 1. Rate constants for the reactions $C^+ + Br^-$ and $C^+ + I^-$ were obtained as upper bounds, where all rate constants up to the reported value gave similar quality fits to data. It was possible to assign a numerical value to the rate constant for the reaction $C^+ + Cl^-$. If we assume that the entirety of the CCl^+ product in Fig. 2(a) comes from the associative ionization reaction $C^+ + Cl^- \rightarrow CCl^+ + e^-$, then we can determine an upper bound of 4×10^{-9} cm^3 s^{-1}. The fact that the upper limits for the Br^- and I^- reactions are larger than the measured value for the Cl^- reaction is due to the upper uncertainty limits for the Ar^+ MN rate constants with Br^- and I^- being larger than that for Cl^-. We note that rate constants for reactions involving rare gas cations and H^+ with atomic halide anions demonstrated a trend $k_{Cl^-} < k_{Br^-} < k_{I^-}$.[24-26]

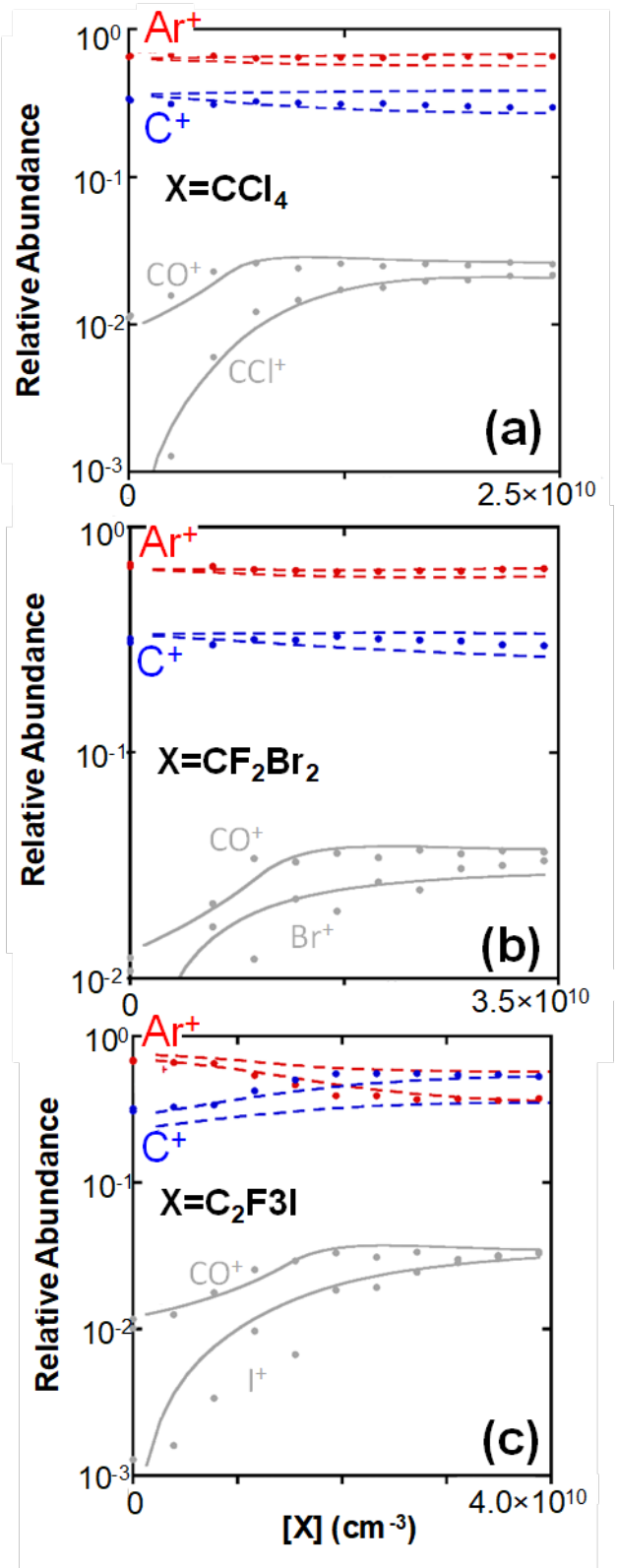

FIG. 2. Relative cation abundances for measurement of a) $C^+ + Cl^-$, b) $C^+ + Br^-$, and c) $C^+ + I^-$ as a function of neutral precursor concentration (points). Dashed lines depict the uncertainty limits

for derived $C^+ + X^-$ rate constant from Monte Carlo simulations. Note that only an upper bound was obtained for $C^+ + Br^-/I^-$ but for ease of interpretation a lower bound corresponding to a rate constant of ~1×10^{-12} cm^{-3} is also shown for these data sets.

TABLE 1. Derived rate constants from the FALP measurements with uncertainty bounds for the indicated $C^+ + X^-$ reaction at 300 K.

	$k\ (10^{-9}\ cm^3\ s^{-1})$		
	Cl^-	Br^-	I^-
C^+	4.2 ± 1.1	< 7.5	< 12.4

Theory

The cross section and thermal rate constant were calculated for mutual neutralization in Cl^- and C^+ collisions. Because Cl has fewer electrons than Br and I, the Cl^- + C^+ system offers the best possibility for a theoretical treatment. In this section, a brief summary of the calculation method is presented, but a more detailed description can be found in a previous work.[29]

The relevant adiabatic potential energy curves and non-adiabatic coupling elements were obtained by performing *ab initio* electronic structure calculations on the CCl molecular system. As a first step, molecular orbitals were obtained using a multi-configuration self-consistent field method (MCSCF) on the CCl ground state (X $^2\Pi$). The basis sets were (16s, 13p, 5d) contracted to [10s, 9p, 5d] for Cl[40] and (11s, 7p, 2d) contracted to [7s, 5p, 2d] for C.[41] In the MCSCF calculation the 6 lowest orbitals, composed of the 1s, 2s, 2p atomic orbitals of Cl and 1s for C, were doubly occupied and an active space of 11 electrons in 8 molecular orbitals (composed of the 3s, 3p atomic orbitals for Cl and 2s, 2p for C) was used. This was followed by a MRCI calculation where the reference configurations were generated using the same active space and single external excitations out of the reference configurations were included.

The incoming ion-pair channel has either $^2\Sigma^+$ or $^2\Pi$ symmetries, which implies that transitions driven by the non-adiabatic coupling are only allowed between electronic states in these symmetries. The adiabatic potential energy curves for the 5 lowest electronic states in $^2\Sigma^+$ symmetry and the 7 lowest states in $^2\Pi$ symmetry were calculated and are displayed in Fig 3. All avoided crossings occur at relatively small internuclear distances (R < 6 a_0). The radial non-adiabatic couplings $F_{ij} = \langle \phi_i | \frac{\partial}{\partial R} | \phi_j \rangle$ among these states were also calculated, and couplings to higher electronic states were assumed to be negligible.

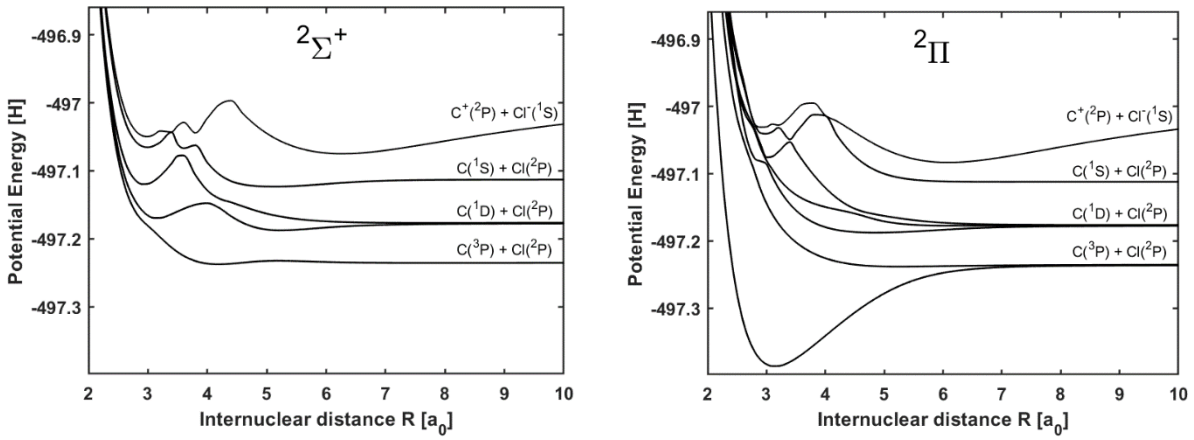

FIG. 3. Adiabatic potential energy curves for the 5 lowest states of CCl in $^2\Sigma^+$ symmetry and the 7 lowest states in $^2\Pi$ symmetry.

Previous studies of CCl are sparse and the potential energy curves have been computed before, but only for the lowest lying states and for smaller internuclear distances.[42-45] Experimentally measured spectroscopic constants are available[46] for the ground state of CCl. These include the equilibrium internuclear distance R_e=1.645 Å, the harmonic and anharmonic vibrational constants ω_e=866.72 cm^{-1} and $\omega_e x_e$ =6.2 cm^{-1} and the dissociation energy D_0=3.47 eV.[46, 47]. More recent measurements[48] and calculations[49, 50] of the heat of formation of CCl implies a dissociation energy of D_0= 4.15 ± 0.01 eV.[51] Our calculation without the inclusion of the spin-orbit interaction yield, for the ground state ($X^2\Pi$) in Fig 3, R_e=1.66 Å, ω_e=858.57 cm^{-1}, $\omega_e x_e$ =4.2 cm^{-1} and D_0=3.99 eV. For the two lowest lying $^2\Sigma^+$ states the harmonic vibrational constants are ω_e=324.6 cm^{-1} for $1^2\Sigma^+$ and ω_e=845.0 cm^{-1} for $2^2\Sigma^+$. These can be compared to values 469 cm^{-1} and 757 cm^{-1} for $1^2\Sigma^+$ and $2^2\Sigma^+$ respectively, previously reported from theoretical calculations of adiabatic potential energy curves.[45]

The nuclear motion of the system was solved in a diabatic representation of the Schrödinger equation. In a strictly diabatic basis all components on the non-adiabatic couplings vanish[52] and the couplings between electronic states are represented by the off-diagonal elements of the diabatic potential matrix. The adiabatic to diabatic transformation matrix **T** were obtained by solving the equation $(\frac{d}{dR} + \boldsymbol{F})\mathbf{T} = 0$, where **F** is the radial non-adiabatic coupling in matrix notation. This equation was solved numerically with a matrix version of the Runge-Kutta Fehlberg method[53] and by imposing the boundary condition **T** = **1** at the internuclear distance R = 10 a_0.

By a partial wave expansion of the nuclear wave function, the coupled radial Schrödinger equation for a given rotational quantum number l was obtained. The scattering matrix and the partial cross section were extracted by matching the asymptotic solution of the radial Schrödinger equation to a linear combination of incoming and outgoing waves. By introducing the logarithmic derivative of the radial wavefunction, the numerically more stable matrix Riccati equation[54, 55] was obtained.

This equation was integrated numerically from R=1.5 a_0 to 30 a_0 where the partial cross sections were extracted. The total neutralization cross section was obtained by summing the partial cross sections over rotational quantum numbers l. The cross section was calculated for collision energies between 0.001 eV and 100 eV. At low energies, 200 partial waves had to be included to converge the cross section, while at higher energies up to 1400 partial waves were included.

The calculated total cross section for mutual neutralization in $Cl^- + C^+$ collisions is shown in Fig. 4 with the red dashed curve. For lower collision energies the cross section shows a characteristic E^{-1} dependence that can be expected for reactions which are governed by the Coulomb interaction.[56] There are some resonant structures in the cross section that are displayed in the inset of Fig 4. These resonances are associated with high rotational quantum numbers around l = 170 and similar resonant structures have been found for mutual neutralization in $H^+ + F^-$ collisions[30] and it is found that they are present in mutual neutralization reactions driven by non-adiabatic couplings at relatively small internuclear distances.

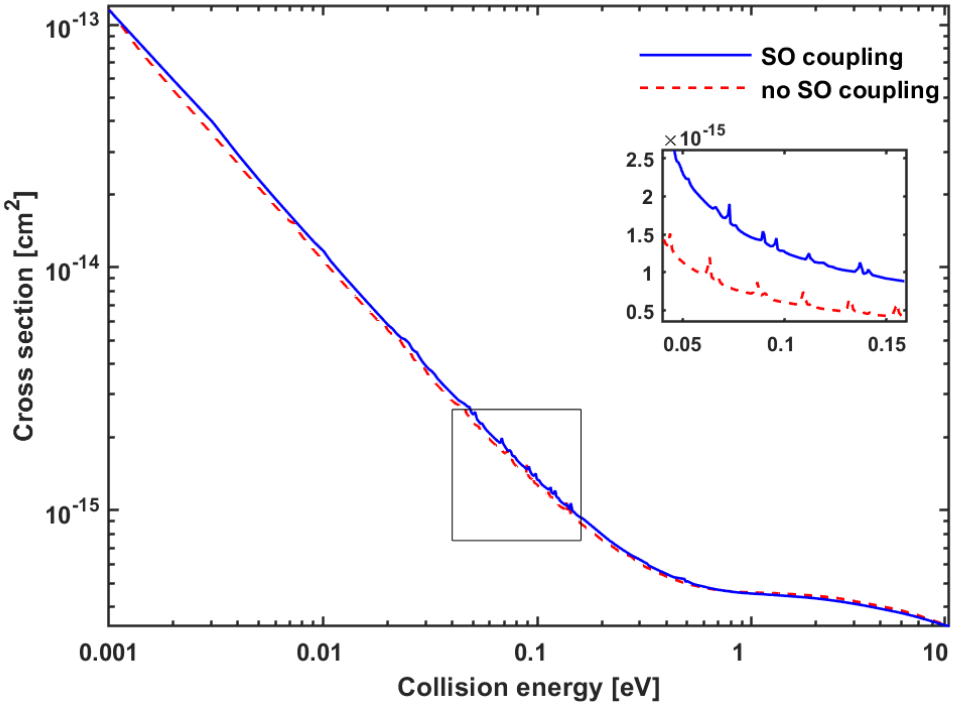

FIG. 4. Total cross section for mutual neutralization in $Cl^- + C^+$ collisions calculated with and without inclusion of spin-orbit interaction using the semi-empirical method described in the text. The inset shows resonance structures in the cross section associated with high rotational quantum numbers.

The thermal rate constant can be calculated by integrating the cross section times the relative velocity v over a Maxwell-Boltzmann velocity distribution. For comparison, at T = 300 K, a thermal rate constant of 3.6×10^{-10} cm^3 s^{-1} was obtained without inclusion of spin-orbit interaction. Compared to the measured value this is about an order of magnitude smaller.

Due to the presence of the Cl atom in the system, spin-orbit (SO) coupling may play a significant role in the reaction.[57,58] To estimate this effect on the reaction rate we have employed a semi-empirical model[35, 36], where the SO strength parameter is assumed to be independent of the internuclear distance and determined by the observed energy splitting of the separated atoms. In our approximation only the $3p^5$ (p-hole) configuration in Cl give rise to the SO-coupling, where the experimental energy level splitting between the $^2P_{1/2}$ and $^2P_{3/2}$ levels of Cl is 0.1094 eV.[59] The SO coupling matrix have been derived by consecutive angular momentum addition from atomic basis to molecular basis.[35]

Since the spin-orbit interaction induces couplings between states with equal quantum number Ω (projection of total angular momentum), we have to include the doublet and quintet electronic states in all symmetries associated with the separated atomic limit considered in the model. Hence, we have in addition to the five $^2\Sigma^+$ and seven $^2\Pi$ potential energy curves also calculated three $^2\Sigma^-$, three $^2\Delta$, one $^2\Phi$ states as well as one $^4\Sigma^+$, two $^4\Sigma^-$, two $^4\Pi$ and one $^4\Delta$ states. These states have to be included in order to construct the hermitian spin-orbit coupled Hamiltonian in a diabatic representation. Only non-adiabatic couplings among the $^2\Sigma^+$ and $^2\Pi$ states were considered. In total a family of 23 states with Ω=1/2 and 16 states with Ω=3/2 were included in the diabatization and scattering calculation. The SO-effect was found to increase the total MN cross section as displayed in Fig. 4. At a collision energy of 0.01 eV, the MN cross section increased by 7.8 %. The thermal rate constant, including SO was found to be 3.9×10^{-10} cm^3 s^{-1}. Thus, inclusion of the spin-orbit coupling cannot account for the discrepancy between theory and experiment.

Discussion

The theoretical 300 K rate constant for $C^+ + Cl^-$ of 3.9×10^{-10} cm^3 s^{-1} is roughly an order of magnitude smaller than the experimentally obtained value of $4.2 \pm 1.1 \times 10^{-9}$ cm^3 s^{-1}. This discrepancy could not be explained by including spin-orbit interactions, which increases the calculated rate constant by just 5%. The effect of autoionization and Penning ionization were not considered in the theoretical model because it is not energetically allowed. Previous studies on $H^+ + F^-$ [30] showed that autoionization was significant for a system where the MN reaction is driven by non-adiabatic interactions occurring at small distances.

In the experiment, total loss of C^+ is measured, which may be a consequence of either mutual neutralization or associative ionization, while the theoretical treatment considers only mutual neutralization. Associative ionization yields CCl^+ and is probed in the experiment by the increase in CCl^+ abundance; however, only an upper limit on the contribution of associative ionization may be set due to the uncertainty in the amount of CCl^+ formed through ion-molecule reactions, e.g. $Ar^+ + CCl_2$, which are challenging to probe experimentally and for which no experimental data exists. That upper bound is ~4×10^{-9} cm^3 s^{-1}, similar to the total rate constant for C^+ loss. Associative ionization cannot be ruled out as accounting for the majority of the experimentally measured rate constant, possibly explaining the order-of-magnitude discrepancy between the measured and calculated rate constants.

Associative ionization cross sections measured using merged beam techniques have been reported for N^+ and $O^+ + O^-$ and for various isotopomers of $H^+ + H^-$ and $He^+ + H^-$.[16, 18, 19, 60] In all cases, the energy dependence of the associative ionization cross sections is stronger than that for the

competing MN pathway such that the contribution of associative ionization is largest at low collision energies. For the systems involving only light atoms, the associative ionization cross section is <1% of the MN cross section at thermal energies, while for the heavy atom systems $N^+ + O^-$ and $O^+ + O^-$ associative ionization cross sections are somewhat larger, but still only 1-2% of MN cross sections at thermal energies. Reconciling the $C^+ + Cl^-$ experiment and theory presented here would require the associative ionization channel cross section to be a factor of 10 *higher* than the MN cross section, seemingly unlikely in light of the literature data unless the system is qualitatively distinct from those studied previously.

An estimate of maximum cross sections for MN and associative ionization has been derived by relating a maximum impact parameter to the internuclear distance at which the reactant Coulomb potential crosses the relevant product channel asymptote, with the resulting upper limits in good agreement with experimental results.[19] For the $C^+ + Cl^-$ system, where associative ionization is exothermic by ~2.2 eV, the estimated maximum rate constant at 300 K is 3.5×10^{-9} cm^3 s^{-1}. While this is the magnitude of rate constant required to reconcile the experiment and theory, it is unlikely that associative ionization occurs at this limit.

There is reason to expect that product branching fraction of associative ionization in the $C^+ + Cl^-$ system is greater than in the previously studied N^+ and $O^+ + O^-$ reactions. MN in those reactions is dominated by production of highly excited neutral species where product exothermicities are just 1 – 3 eV, well under the exothermicities of the associative ionization channels.[18] In the $C^+ + Cl^-$ system, fewer MN product channels are available (primarily due to the lack of low-lying states of Cl), and the open states have exothermicities of 4 – 7.6 eV, well above that of the associative ionization channel, and smaller exothermicity implies a larger maximum impact parameter for the channel. The possibility may be evaluated in two ways: one, by theoretical treatment of the associative ionization pathway or, two, experimental study of the $C^+ + Cl^-$ reaction at thermal energies in a merged-beam apparatus with more direct access to product formation.[18, 19]

Conclusions

This work provides an addition to the scarce direct comparisons between theoretical and experimental MN rate constants. Developing *ab initio* and quantum mechanical calculations such as this have been primarily restricted to atom-atom systems with only a few electrons previously. This makes the $C^+ + Cl^-$ the most complex system treated to date, where also the inclusion of spin-orbit interaction has been considered. Thermal rate constants measured using a new variation of the VENDAMS method on AFRL's FALP apparatus provided only an upper bound for the reactions of $C^+ + Br^-, I^-$ but yields a rate constant for the reaction of C^+ with Cl^- at 300 K. The $4.2 \pm 0.4 \times 10^{-9}$ cm^3 s^{-1} experimentally obtained thermal rate constant for $C^+ + Cl^-$ is an order of magnitude larger than the theoretical rate constant of 3.9×10^{-10} cm^3 s^{-1}. Spin-orbit coupling contributions were considered in the theoretical treatment, but only increased the rate constant by 5% from 3.6×10^{-10} cm^3 s^{-1}. The discrepancy may be due to an associative ionization channel (i.e. formation of CCl^+) for which an upper limit of 4×10^{-9} cm^3 s^{-1} (i.e. nearly 100% of product branching) is placed on the experimental results, but has not been included in the theoretical treatment. Estimates suggest that it is possible but unlikely for associative ionization to proceed

this quickly. Alternatively, the experimentally derived value, determined from the C^+-loss rate, could be overestimated due to an unconsidered C^+-loss channel.

Acknowledgements

J.C.S. acknowledges support of the National Research Council. We are grateful for the support of the Air Force Office of Scientific Research for this work under Project AFOSR-19RVCOR042 and 16RVCOR276. T.M.M. is under contract from the institute for Scientific Research of Boston College.

Å.L. acknowledges support from the Swedish research council for this work under project 2014-4164

References

1. N. S. Shuman, D. E. Hunton and A. A. Viggiano, Chem. Rev. **115**, 4542–4570 (2015).
2. A. B. Fialkov, Progress in Energy and Combustion Science **23**, 399-528 (1997).
3. D. Smith, Chem. Rev. **92**, 1473-1485 (1992).
4. D. Smith, N. G. Adams and M. J. Church, Planetary and Space Science **24**, 697-703 (1976).
5. U. Kogelschatz, K. Becker, K. Schoenbach and R. Barker, Plasma Physics, (2004).
6. G. A. Fisk, B. H. Mahan and E. K. Parks, J. Chem. Phys. **47**, 2649 (1967).
7. B. H. Mahan and J. C. Person, J. Chem. Phys. **40**, 392 (1964).
8. T. S. Carlton and B. H. Mahan, J. Chem. Phys. **40**, 3683 (1964).
9. M. N. Hirsh and P. N. Eisner, Radio Sci. **7**, 125 (1972).
10. P. M. Eisner and M. N. Hirsh, Phys. Rev. Lett. **26**, 874 (1971).
11. J. T. Moseley, W. Aberth and J. R. Peterson, J. Geophys. Res. **77**, 255 (1972).
12. J. R. Peterson, W. H. Aberth, J. T. Moseley and J. R. Sheridan, Phys. Rev. A **3**, 1651 (1971).
13. R. E. Olson, J. R. Peterson and J. Moseley, J. Chem. Phys. **53**, 3391 (1970).
14. J. Moseley, W. Aberth and J. R. Peterson, Phys. Rev. Lett. **24**, 435 (1970).
15. D. Smith, M. J. Church and T. M. Miller, J. Chem. Phys. **68**, 1224-1229 (1978).
16. S. M. Nkambule, N. Elander, Å. Larson, J. Lecointre and X. Urbain, Phys. Rev. A **93**, 032701 (2016).
17. X. Urbain, J. Lecointre, F. Mezdari, K. A. Miller and D. W. Savin, XXVII International Conference on Photonic, Electronic and Atomic Collisions (Icpeac 2011), Pts 1-15 **388**, 092004 (2012).
18. N. de Ruette, A. Dochain, T. Launoy, R. F. Nascimento, M. Kaminska, M. H. Stockett, N. Vaeck, H. T. Schmidt, H. Cederquist and X. Urbain, Phys. Rev. Lett. **121**, 083401 (2018).
19. A. L. Padellec, T. Launoy, A. Dochain and X. Urbain, J. Phys. B: At., Mol. Opt. Phys. **50**, 095202 (2017).
20. N. S. Shuman, T. M. Miller, A. A. Viggiano and J. Troe, Adv. Atom. Mol. Opt. Phys. **61**, 209-294 (2012).
21. N. S. Shuman, J. P. Wiens, T. M. Miller and A. A. Viggiano, J. Chem. Phys. **140**, 224309 (2014).
22. T. M. Miller, N. S. Shuman and A. A. Viggiano, J. Chem. Phys. **136**, 204306 (2012).
23. N. S. Shuman, T. M. Miller, N. Hazari, E. D. Luzik and A. A. Viggiano, J. Chem. Phys. **133**, 234304 (2010).
24. J. C. Sawyer, T. M. Miller, B. C. Sweeny, S. G. Ard, A. A. Viggiano and N. S. Shuman, J. Chem. Phys. **149**, 044303 (2018).
25. J. P. Wiens, N. S. Shuman, T. M. Miller and A. A. Viggiano, J. Chem. Phys. **144**, 204309 (2016).
26. N. S. Shuman, T. M. Miller, R. Johnsen and A. A. Viggiano, J. Chem. Phys. **140**, 044304 (2013).
27. H. Croft, A. S. Dickinson and F. X. Gadéa, J. Phys. B: At., Mol. Opt. Phys. **32**, 81 (1999).
28. A. S. Dickinson, R. Poteau and F. X. Gadéa, J. Phys. B: At., Mol. Opt. Phys. **32**, 5451 (1999).
29. M. Stenrup, Å. Larson and N. Elander, Phys. Rev. A **79**, 012713 (2009).
30. J. Z. Mezei, J. B. Roos, K. Shilyaeva, N. Elander and Å. Larson, Phys. Rev. A **84**, 012703 (2011).

31. A. K. Belyaev, P. S. Barklem, A. Spielfiedel, M. Guitou, N. Feautrier, D. S. Rodionov and D. V. Vlasov, Phys. Rev. A **85**, 032704 (2012).
32. M. Guitou, A. Spielfiedel, D. S. Rodionov, S. A. Yakovleva, A. K. Belyaev, T. Merle, F. Thévenin and N. Feautrier, Chem. Phys. **462**, 94-103 (2015).
33. Å. Larson, S. M. Nkambule and A. E. Orel, Phys. Rev. A **94**, 022709 (2016).
34. Å. Larson, J. Hornquist and A. E. Orel, J. Chem. Phys., (personal communication).
35. J. S. Cohen and B. Schneider, J. Chem. Phys. **61**, 3230-3239 (1974).
36. P. J. Hay, T. H. Dunning Jr. and R. C. Raffenetti, J. Chem. Phys. **65**, 2679-2689 (1976).
37. N. S. Shuman, T. M. Miller, C. M. Caples and A. A. Viggiano, Abstr. Pap. Am. Chem. Soc. **239**, (2010).
38. D. Smith, N. G. Adams and E. Alge, J. Phys. B-At. Mol. Opt. Phys. **17**, 461-472 (1984).
39. N. S. Shuman, J. F. Friedman, T. M. Miller and A. A. Viggiano, J. Chem. Phys. **137**, 164306 (2012).
40. A. D. McLean and G. S. Chandler, J. Chem. Phys. **72**, 5639-5648 (1980).
41. T. H. Dunning Jr., J. Chem. Phys. **53**, 2823-2833 (1970).
42. M. Bialski and F. Grein, J. Mol. Spectrosc. **61**, 321-331 (1976).
43. M. Larsson, M. R. A. Blomberg and P. E. M. Siegbahn, Mol. Phys. **46**, 365-382 (1982).
44. S. Karna and F. Grein, Int. J. Quantum Chem. **29**, 755-766 (1986).
45. Y. Li and J. S. Francisco, J. Chem. Phys. **114**, 2192-2196 (2001).
46. K. P. Huber and G. Herzberg, NIST chemistry webBook, NIST standard reference database, 20899 (2000).
47. V. Vedeneyev, L. V. Gurvich, V. Kondrat'Yev, V. Medvendev and Y. L. Frankevich, *Bond energies, ionization potentials, and electron affinities*. (E. Arnold London, 1966).
48. S. S. Kumaran, M. C. Su, K. P. Lim, J. V. Michael, S. J. Klippenstein, J. DiFelice, P. S. Mudipalli, J. H. Kiefer, D. A. Dixon and K. A. Peterson, J. Phys. Chem. A **101**, 8653-8661 (1997).
49. D. A. Dixon and K. A. Peterson, J. Chem. Phys. **115**, 6327-6329 (2001).
50. J. Csontos, Z. Rolik, S. Das and M. Kallay, J. Phys. Chem. A **114**, 13093-13103 (2010).
51. B. Ruscic and D. H. Bross, *Active Thermochemical Tables (ATcT) based on ver. 1.122 of the Thermochemical Network (2016); available at ATcT.anl.gov* https://atct.anl.gov acessed: January 29, 2019.
52. C. A. Mead and D. G. Truhlar, J. Chem. Phys. **77**, 6090-6098 (1982).
53. W. Cheney and D. Kincaid, WH Press and S. A. Teukolsky, Comput. Phys **6**, 188 (1992).
54. B. R. Johnson, *Multichannel log-derivative method for scattering calculations*, (1973).
55. B. Johnson, Phys. Rev. A **32**, 1241 (1985).
56. E. P. Wigner, Phys. Rev. **73**, 1002 (1948).
57. X. Zhang, H. Zhai, Y. Liu and J. Sun, Journal of Quantitative Spectroscopy and Radiative Transfer **119**, 23-31 (2013).
58. D. Khiri, M. Hochlaf, G. Maroulis and G. Chambaud, J. Phys. Chem. A **122**, 2353-2360 (2018).
59. A. Kramida, Y. Ralchenko and J. Reader, *NIST Atomic Spectra Database (ver 5.3), [Online]. Available: http://physics.nist.gov/asd [2018, April 1]*. (National Institue of Standards and Technology, Gaithersburg, MD, 2018).
60. T. Nzeyimana, E. A. Naji, X. Urbain and A. Le Padallec, Eur. Phys. J. D **19**, 315-325 (2002).